Insights into catalytic reforming from a new oscillating reaction

Yu Zhang[1,2], Qian Wang[2], Peter Glarborg[1], Martin P. Andersson[3], Jakob B. Wagner[4], Keld Johansen[5], Thomas K. Torp[5], Anker D. Jensen[1], Chaofeng Hou[2], Wei Ge[2], Jakob M. Christensen[1]*

Corresponding author: jmc@kt.dtu.dk

Table of contents

Supplementary Figure 1. 4
Supplementary Figure 2. 5
Supplementary Figure 3. 6
Supplementary Figure 4. 7
Supplementary Figure 5. 8
Supplementary Figure 6. 9
Supplementary Figure 7. 10
Supplementary Figure 8. 11
Supplementary Figure 9. 12
Supplementary Figure 10. 13
Supplementary Figure 11. 14
Supplementary Figure 12. 15
Supplementary Figure 13. 16
Supplementary Figure 14. 17
Supplementary Figure 15. 18
Supplementary Figure 16. 19
Supplementary Figure 17. 20
Supplementary Figure 18. 21
Supplementary Figure 19. 22
Supplementary Figure 20. 23
Supplementary Figure 21. 24
Supplementary Figure 22. 25
Supplementary Figure 23. 26
Supplementary Figure 24. 27
Supplementary Figure 25. 28
Supplementary Figure 26. 29
Supplementary Figure 27. 30
Supplementary Figure 28. 31
Supplementary Figure 29. 32
Supplementary Figure 30. 33
Supplementary Figure 31. 34
Supplementary Figure 32. 35
Supplementary Table 1. 36
Supplementary Table 2. 37
Supplementary Table 3. 38

Supplementary Note 1..... 39
Supplementary Note 2..... 40
Supplementary Note 3..... 41
Description for Supplementary Movie 1..... 42
Description for Supplementary Movie 2..... 42
Description for Supplementary Movie 3..... 42
Description for Supplementary Movie 4..... 42
Description for Supplementary Movie 5..... 42
Description for Supplementary Movie 6..... 43
Description for Supplementary Movie 7..... 43
Description for Supplementary Movie 8..... 43
Description for Supplementary Movie 9..... 43
Description for Supplementary Movie 10..... 43
Description for Supplementary Movie 11..... 44
Description for Supplementary Movie 12..... 44
Supplementary References..... 44

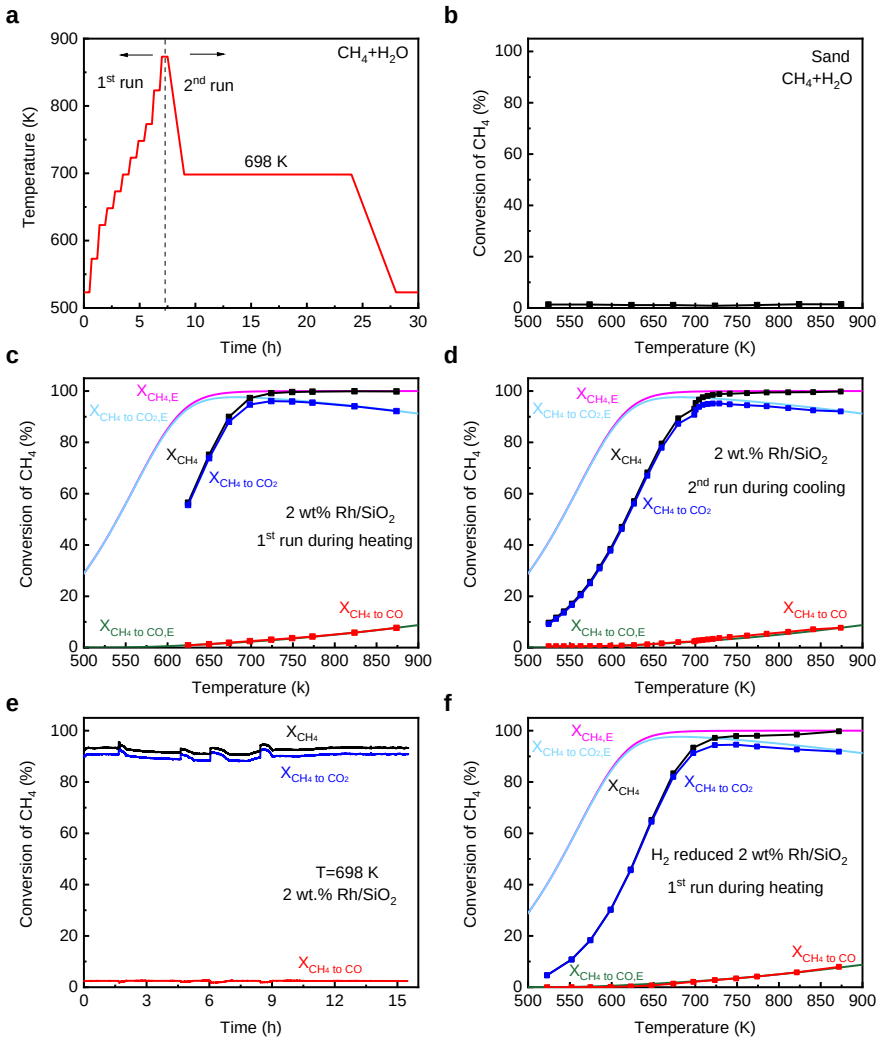

Supplementary Figure 1.

a, Temperature program for the activity test for CH_4 steam reforming. **b,** Activity of pure sand used as dilutant. **c,** Conversion of CH_4 on the non-prereduced 2 wt% Rh/SiO_2 catalyst in the first run during heating. **d,** Conversion of CH_4 on non-prereduced 2wt% Rh/SiO_2 catalyst in the second run during cooling. **e,** Stability of 2 wt% Rh/SiO_2 catalyst at 698 K. **f,** Conversion of CH_4 on the H_2 reduced 2 wt % Rh/SiO_2 catalyst in the first run during heating. H_2 reduction was carried out by in-situ heating to 673 K in N_2 and then reducing in 10 vol% H_2 in N_2 for 1 h. After reduction, the catalyst bed was cooled down to 523 K in the 10 vol% H_2 in N_2 atmosphere and then switching to reforming atmosphere for activity measurement starting at 523 K. Results illustrate that the active phase is the metallic phase that can be produced by H_2 pre-reduction or by the reforming atmosphere at 625 K. The conversion curves with a label marked by '$_E$' are the equilibrium conversions calculated by the HSC Chemistry Software. Test conditions: 2500 ppm CH_4, 5 vol% H_2O, balanced with N_2, GHSV=150,000 NmL/(g_{cat}·h).

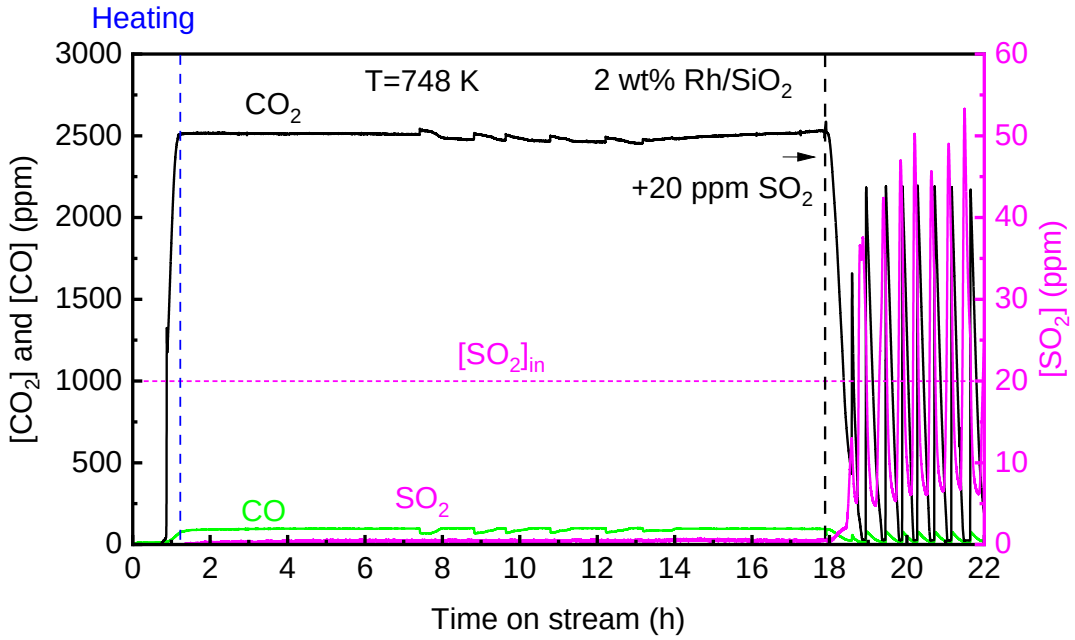

Supplementary Figure 2.

Addition of 20 ppm SO_2 to the reforming reaction gas at 748 K on 2 wt% Rh/SiO_2 catalyst. The magenta dashed line represents the inlet concentration of SO_2 (20 ppm). Test conditions: 2500 ppm CH_4, 5 vol% H_2O, 20 ppm SO_2 when present, balanced with N_2, GHSV=150,000 NmL/(g_{cat}·h).

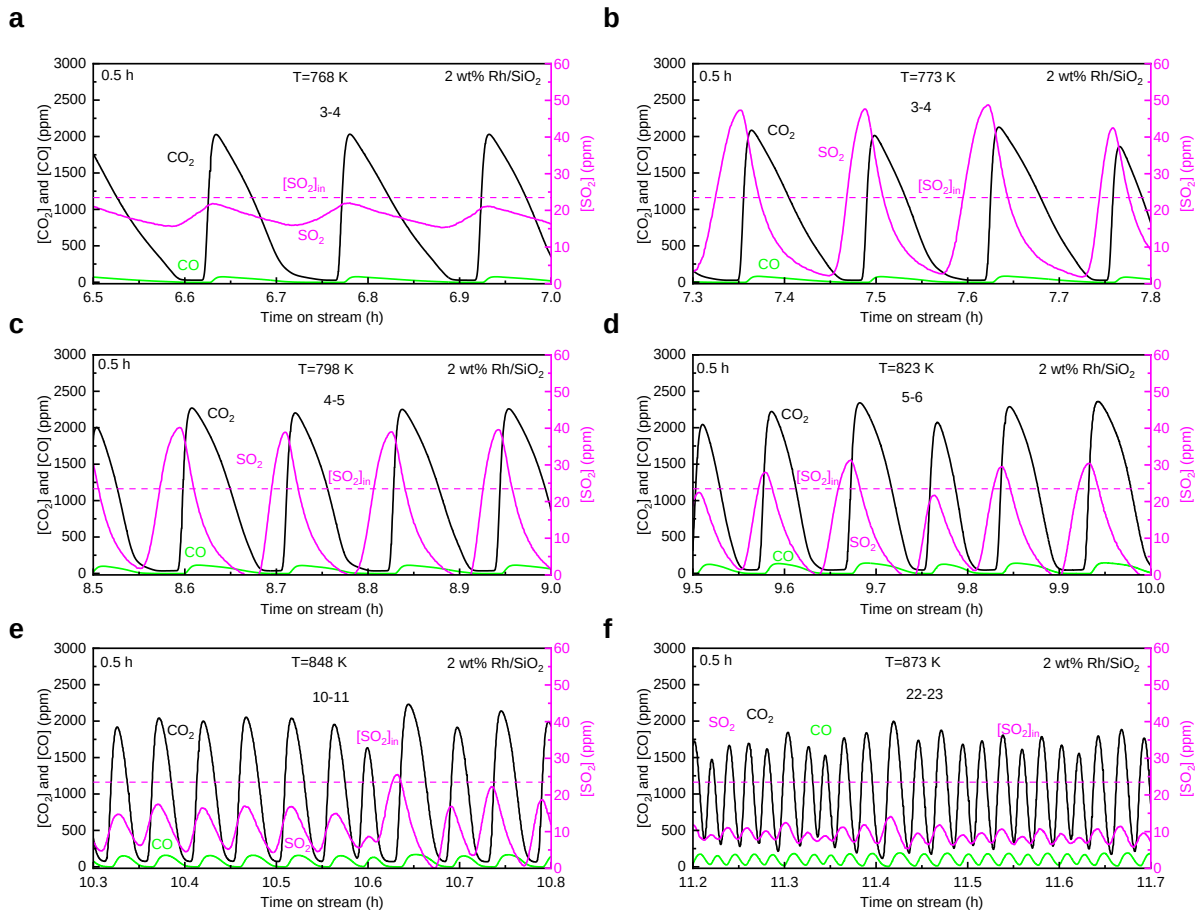

Supplementary Figure 3.

Oscillations on 2 wt% Rh/SiO_2 catalyst during CH_4 steam reforming in the presence of SO_2 at 768 K in **a**, 773 K in **b**, 798 K in **c**, 823 K in **d**, 848 K in **e**, and 873 K in **f**. The oscillation in SO_2 concentration at 768 K in **a** is in a much smaller range compared with that at other temperatures, this was caused by the buffer effect from absorption of SO_2 in condensed water in the outlet tube. The effect could be eliminated by pumping the condensed water out. The magenta dashed lines represent the SO_2 concentration sending to the reactor. The numbers in the middle of the figures denote the number of oscillations counted in the measured 0.5 h. Test conditions: 2500 ppm CH_4, 5 vol% H_2O, 20 ppm SO_2, balanced with N_2, GHSV=150,000 NmL/(g_{cat}·h).

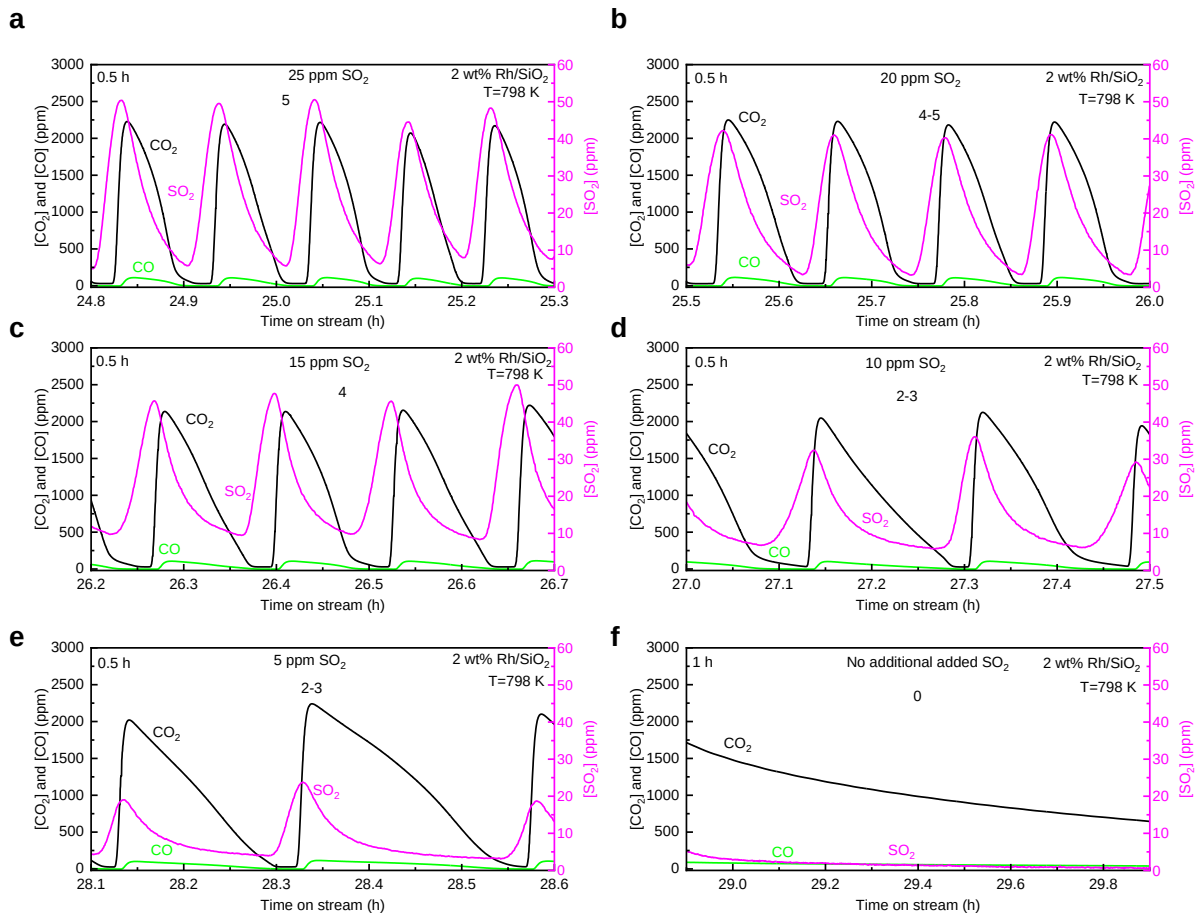

Supplementary Figure 4.

Oscillations on 2 wt% Rh/SiO_2 catalyst at 798 K in the presence of 25 ppm SO_2 in **a**, 20 ppm SO_2 in **b**, 15 ppm SO_2 in **c**, 10 ppm SO_2 in **d**, 5 ppm SO_2 in **e**, and no additional added SO_2 in **f**. The numbers in the middle of the figures denote the number of oscillations counted in the measured 0.5 h. Test conditions: 2500 ppm CH_4, 5 vol% H_2O, 5–25 ppm SO_2 when present, balanced with N_2, GHSV=150,000 Nml/(g_{cat}·h).

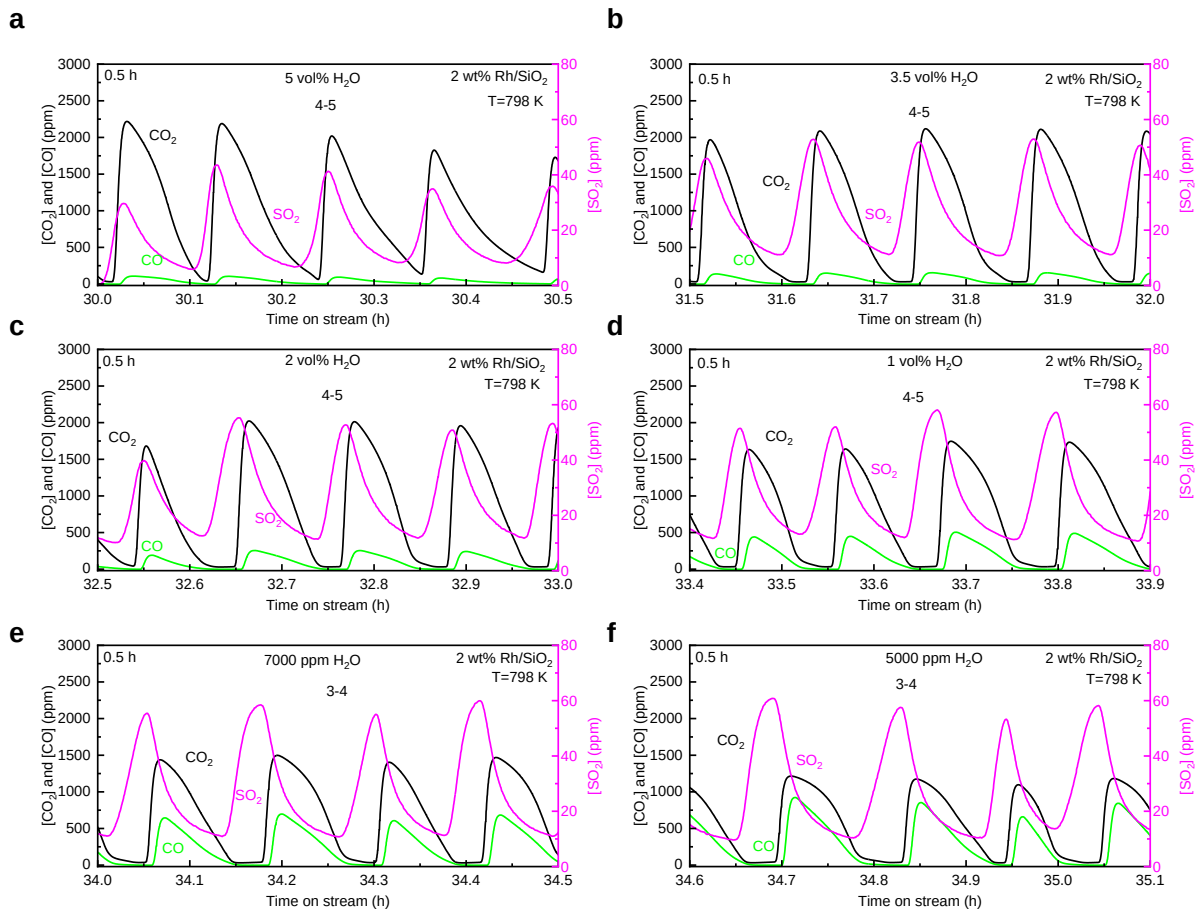

Supplementary Figure 5.

Oscillations on 2 wt% Rh/SiO_2 catalyst at 798 K in the presence of 20 ppm SO_2 at $H_2O/CH_4 \geq 2$. 5 vol% H_2O in **a**, 3.5 vol% H_2O in **b**, 2 vol% H_2O in **c**, 1 vol% H_2O in **d**, 7000 ppm H_2O in e, and 5000 ppm H_2O in **f**. The numbers in the middle of the figures denote the number of oscillations counted in the measured 0.5 h. Test conditions: 2500 ppm CH_4, 5000 ppm–5 vol% H_2O, 20 ppm SO_2, balanced with N_2, GHSV=150,000 Nml/(g_{cat}·h).

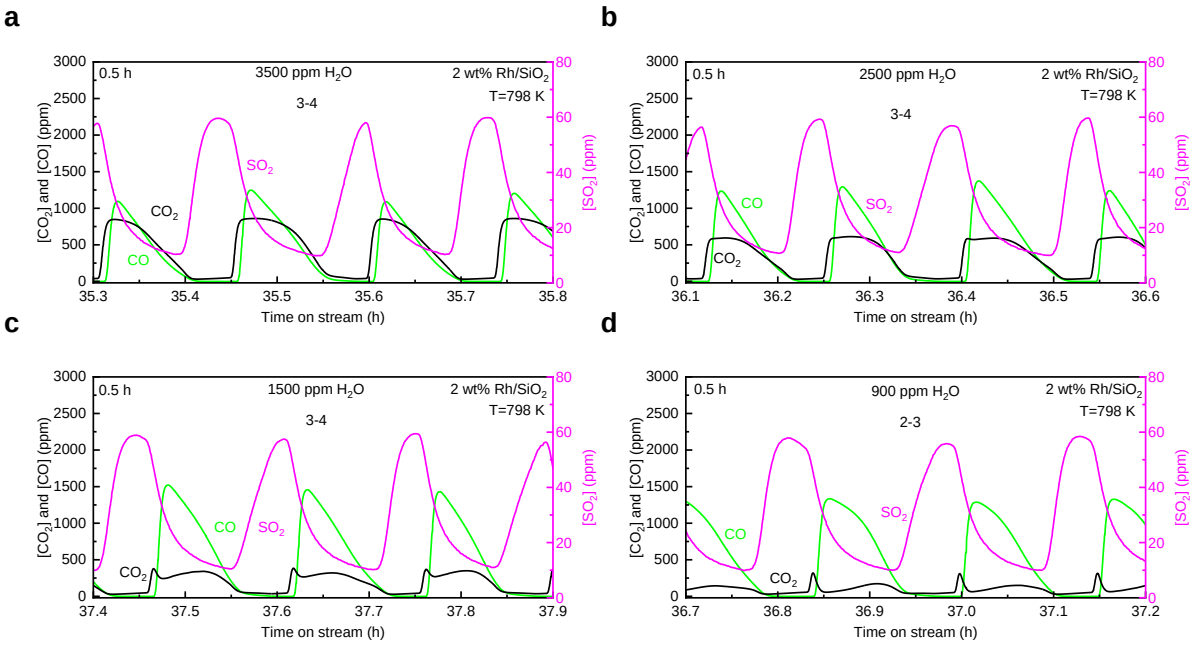

Supplementary Figure 6.

Oscillations on 2 wt% Rh/SiO_2 catalyst at 798 K in the presence of 20 ppm SO_2 at $H_2O/CH_4 < 2$. 3500 ppm H_2O in **a**, 2500 ppm H_2O in **b**, 1500 ppm H_2O in **c**, 900 ppm H_2O in **d**. The numbers in the middle of the figures denote the number of oscillations counted in the measured 0.5 h. Test conditions: 2500 ppm CH_4, 3500–900 ppm H_2O, 20 ppm SO_2, balanced with N_2, GHSV=150,000 Nml/(g_{cat}·h).

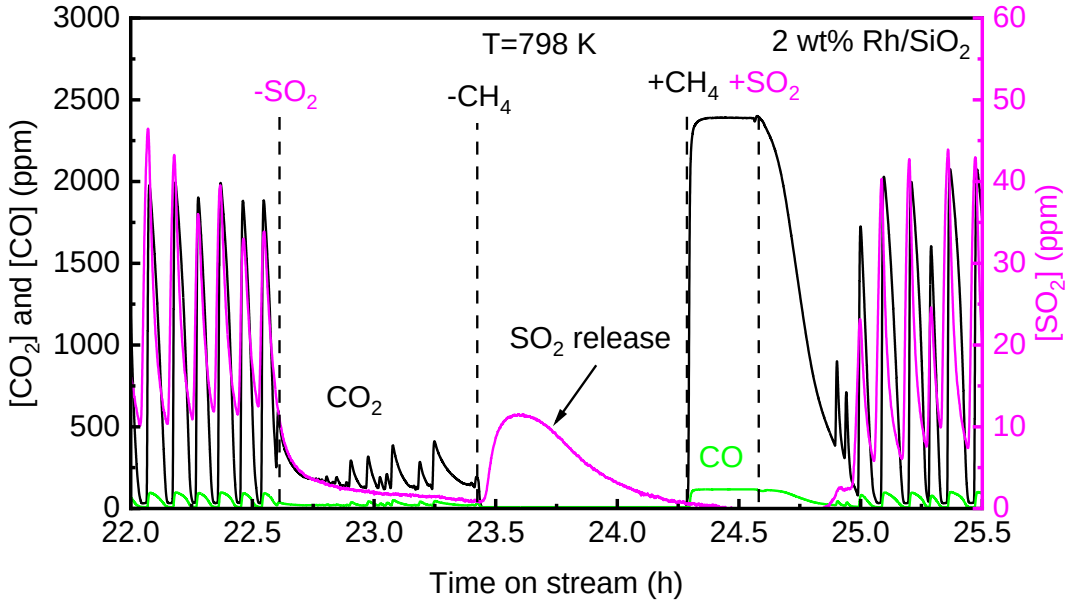

Supplementary Figure 7.

Removal of SO_2 and generation of active state in only H_2O-containing atmosphere. Test conditions: 2500 ppm CH_4 when present, 5 vol% H_2O when present, 20 ppm SO_2 when present, balanced with N_2, GHSV=150,000 Nml/(g_{cat}·h).

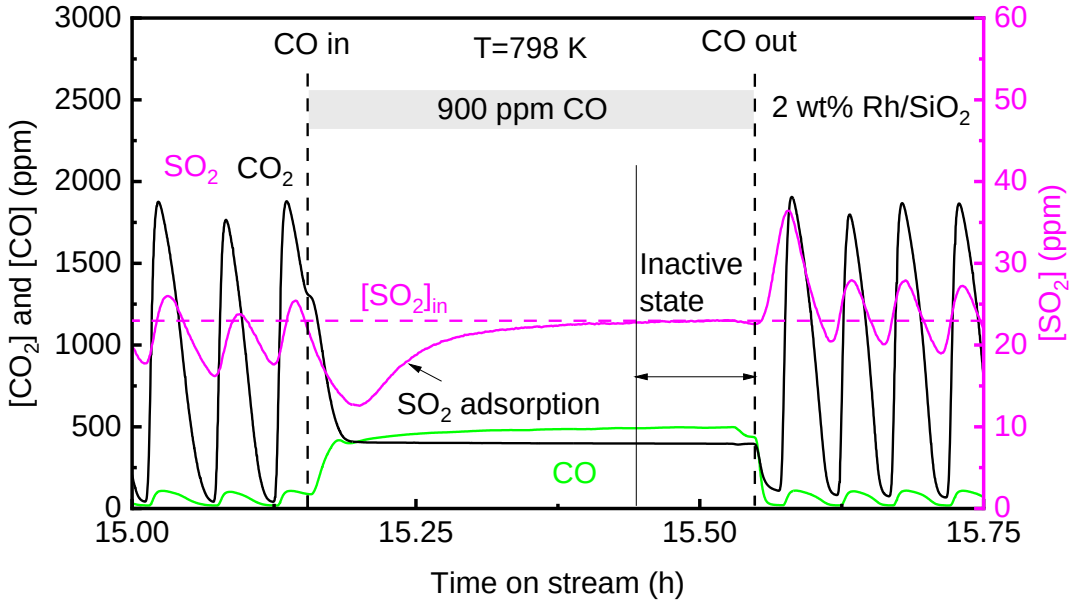

Supplementary Figure 8.

Illustration for the inactive state generated by adding 900 ppm CO into the reaction atmosphere during oscillations. Note the period of SO_2 adsorption upon CO addition and the sulfur release after removing CO followed by recovery of the activity. The presence of CO and CO_2 when CO was present (marked in gray) was attributed to the incomplete conversion of CO to CO_2 via water gas shift reaction. Test conditions: 2500 ppm CH_4, 5 vol% H_2O in, 20 ppm SO_2, 900 ppm CO when present, balanced with N_2, GHSV=150,000 Nml/(g_{cat}·h).

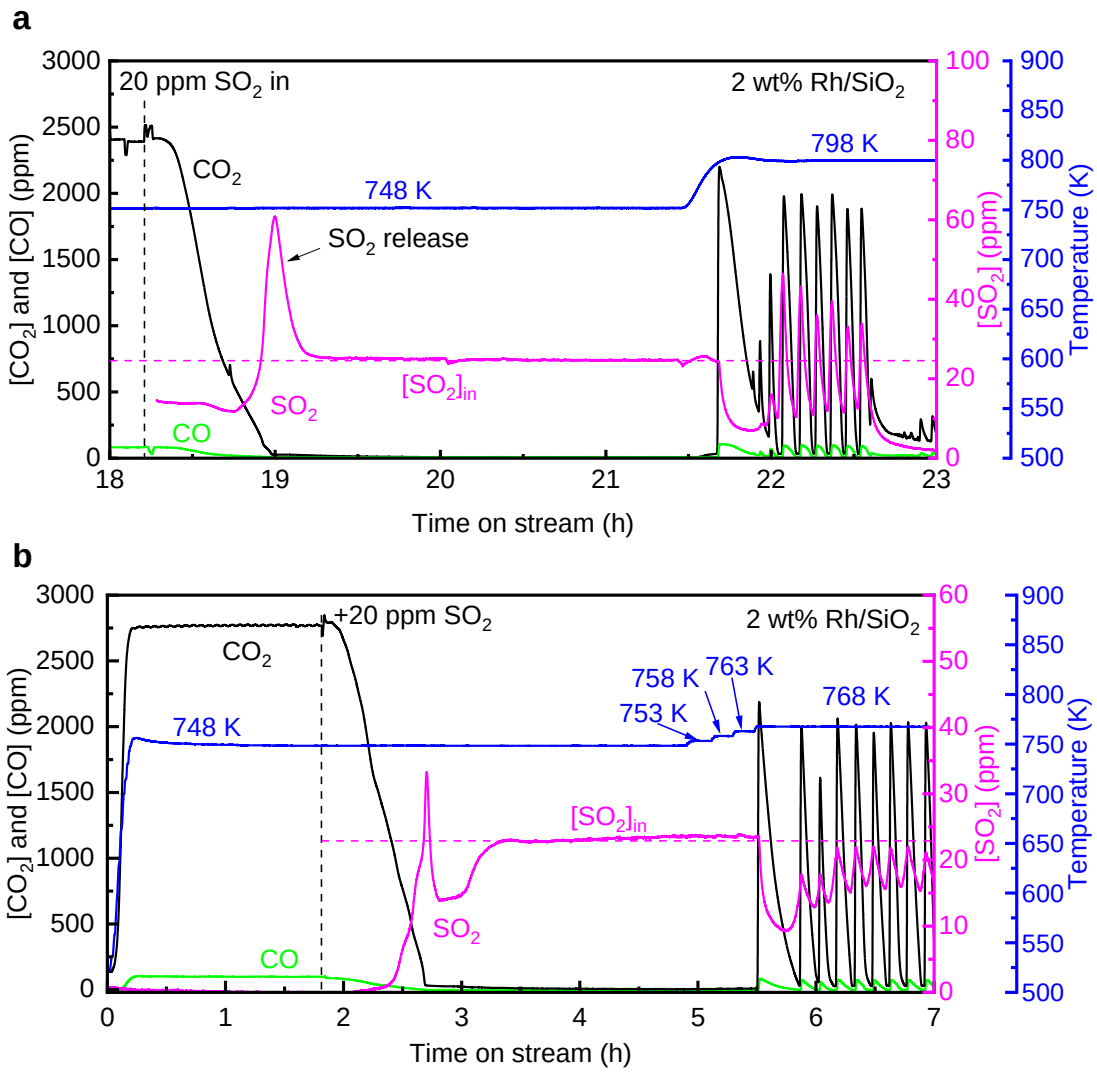

Supplementary Figure 9.

a, Start of the oscillations during heating from 748 to 798 K in the presence of 20 ppm SO_2, illustrating the need for thermal energy to initiate the oscillations. The activity in 0-18 h was stable and is not shown in the figure. **b,** Addition of 20 ppm SO_2 at 748 K to the reforming atmosphere following by heating to 768 K with a temperature increment of 5 K. Catalyst: 2 wt% Rh/SiO_2. The magenta dash line represents the inlet SO_2 concentration measure by the SO_2 analyzer. Test conditions: 2500 ppm CH_4, 5 vol% H_2O, 20 ppm SO_2 when present, balanced with N_2, GHSV=150,000 NmL/(g_{cat}·h). The oscillation in SO_2 concentration in **b** was always lower than the inlet SO_2 concentration due to the buffer effect of the condensed water in the outlet tube and this buffer effect can be avoided by removing the condensed water by a pump as shown in Supplementary Fig. 3.

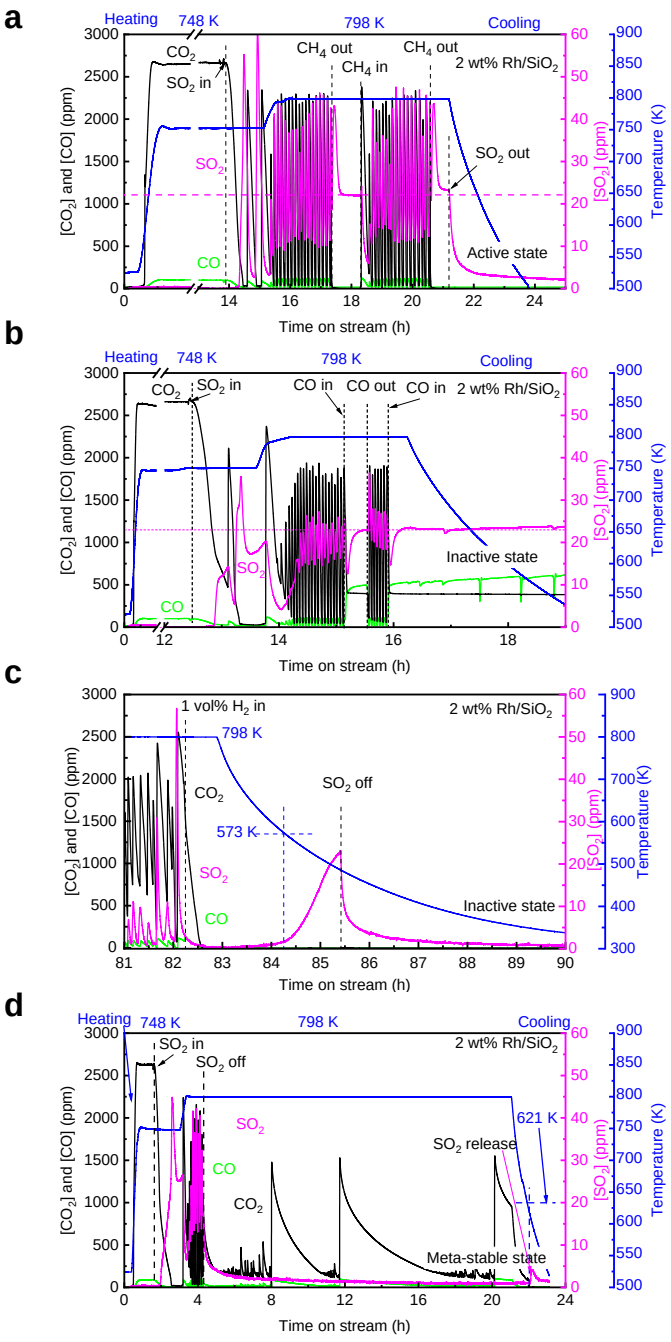

Supplementary Figure 10.

Preparation of ex-situ catalysts at different states. **a,** Active sate by cooling in CH_4-free gas. **b,** Inactive state by cooling after addition of 900 ppm CO. **c,** Inactive state by cooling after addition of 1 vol% H_2. **d,** Meta-stable state by cooling in CH_4+H_2O atmosphere after removal of SO_2. The magenta dash lines in **a** and **b** represent the inlet SO_2 concentrations. Test conditions: 2500 ppm CH_4 when present, 5 vol% H_2O, 20 ppm SO_2 when present, 900 ppm CO when present, balanced with N_2, GHSV=150,000 NmL/(g_{cat}·h).

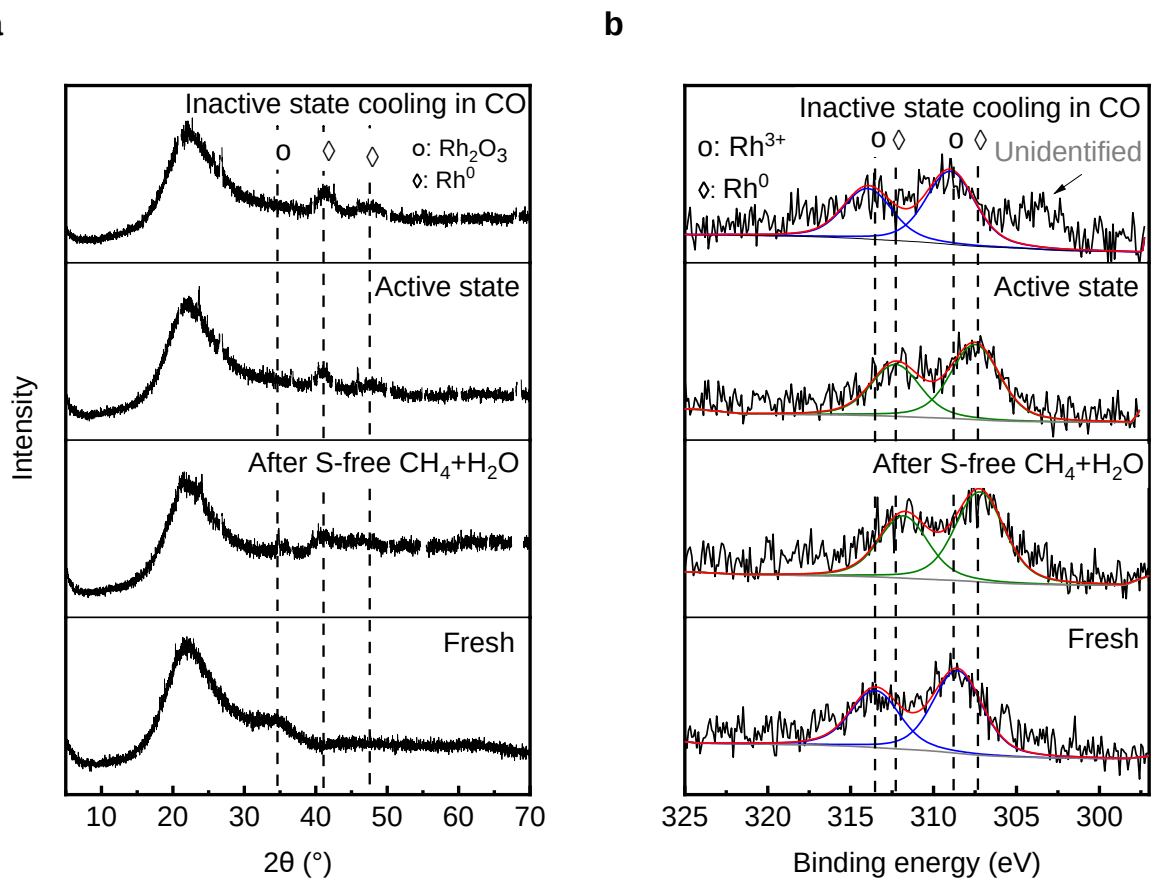

Supplementary Figure 11.

XRD in **a** and XPS in **b** analyses of fresh and spent 2 wt% Rh/SiO_2 catalysts: fresh catalyst, spent after S-free CH_4+H_2O, active state prepared by cooling after removal of CH_4 during fluctuation at 798 K as shown in Supplementary Fig. 10a, and inactive state prepared by cooling after addition of 900 ppm CO during fluctuation at 798 K as shown in Supplementary Fig. 10b. The circle and diamonds in **a** represent Rh_2O_3 oxide and metallic Rh respectively, the circles and diamonds in **b** marks the binding energies for Rh^{3+} and Rh^0. The unidentified XPS peak for inactive state was caused by the pollution of the XPS sample holder.

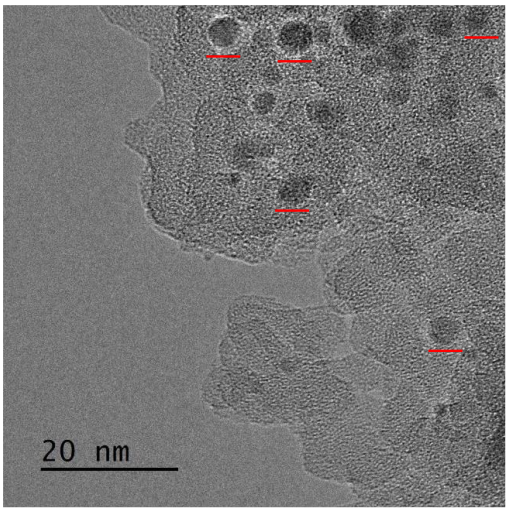

Supplementary Figure 12.

TEM images of active state of 2 wt% Rh/SiO_2 catalysts prepared from Fig.S10a. The red lines in the images represent 5 nm. The TEM image of inactive states of 2 wt% Rh/SiO_2 catalyst is shown in Fig. 2c in the main text. The TEM images of active and inactive states of 2 wt% Rh/SiO_2 catalysts shows no significant difference in the morphology of the two states. The Rh nanoparticle size was around 5 nm at both states.

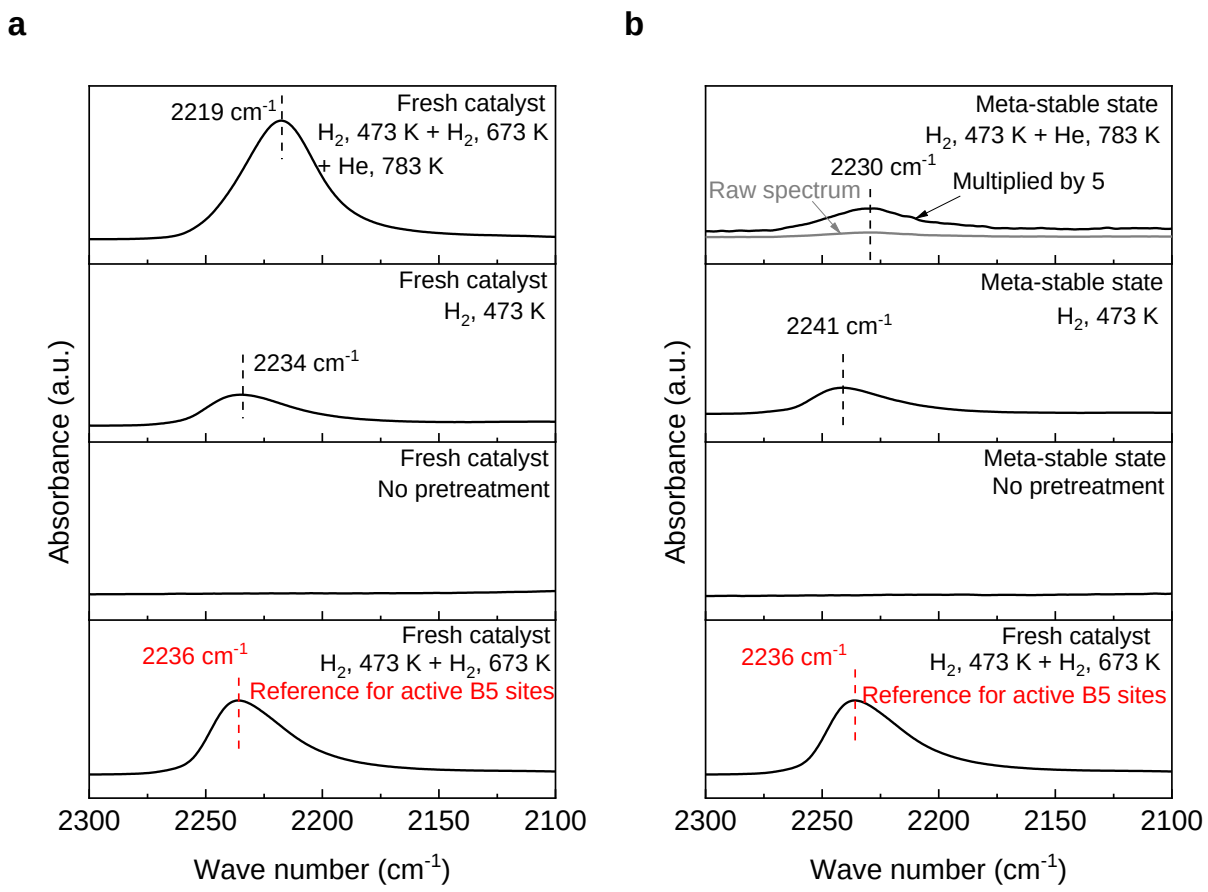

Supplementary Figure 13.

DRIFTS spectra of N_2 chemisorbed on fresh 2 wt% Rh/SiO_2 catalyst in **a** and 2 wt % Rh/SiO_2 catalyst at meta-stable state prepared by cooling after removal of SO_2 from the oscillation atmosphere as shown in Supplementary Fig. 10d in **b**. The spectra of H_2 reduced fresh 2 wt% Rh/SiO_2 catalyst was shown in both figures as a reference for the N_2 chemisorption on the active B5 sites.

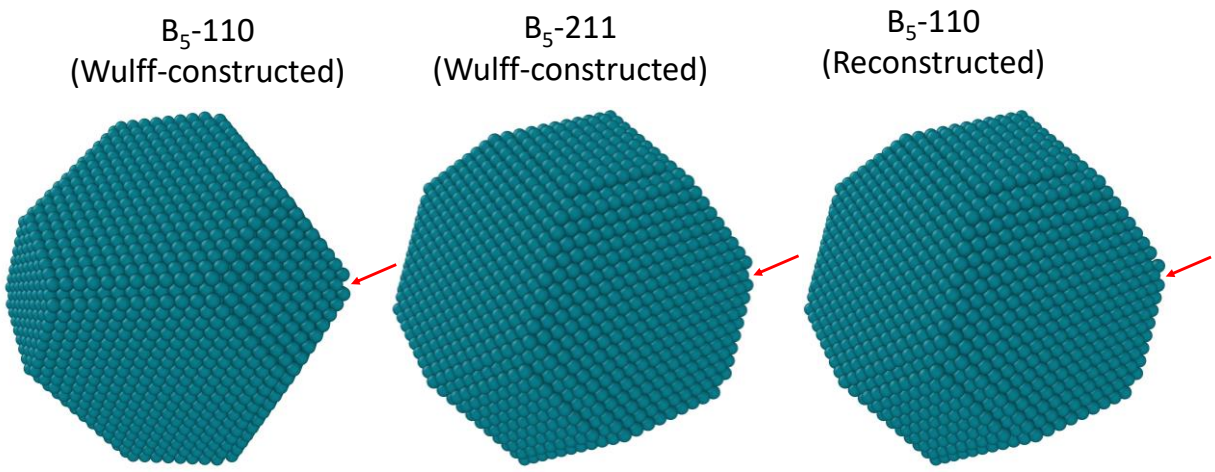

Supplementary Figure 14.

Illustrations for edge of Wulff-constructed B_5-110 and B_5-211 steps, and reconstructed B_5-110 step. The red arrows point to the edge of the particles.

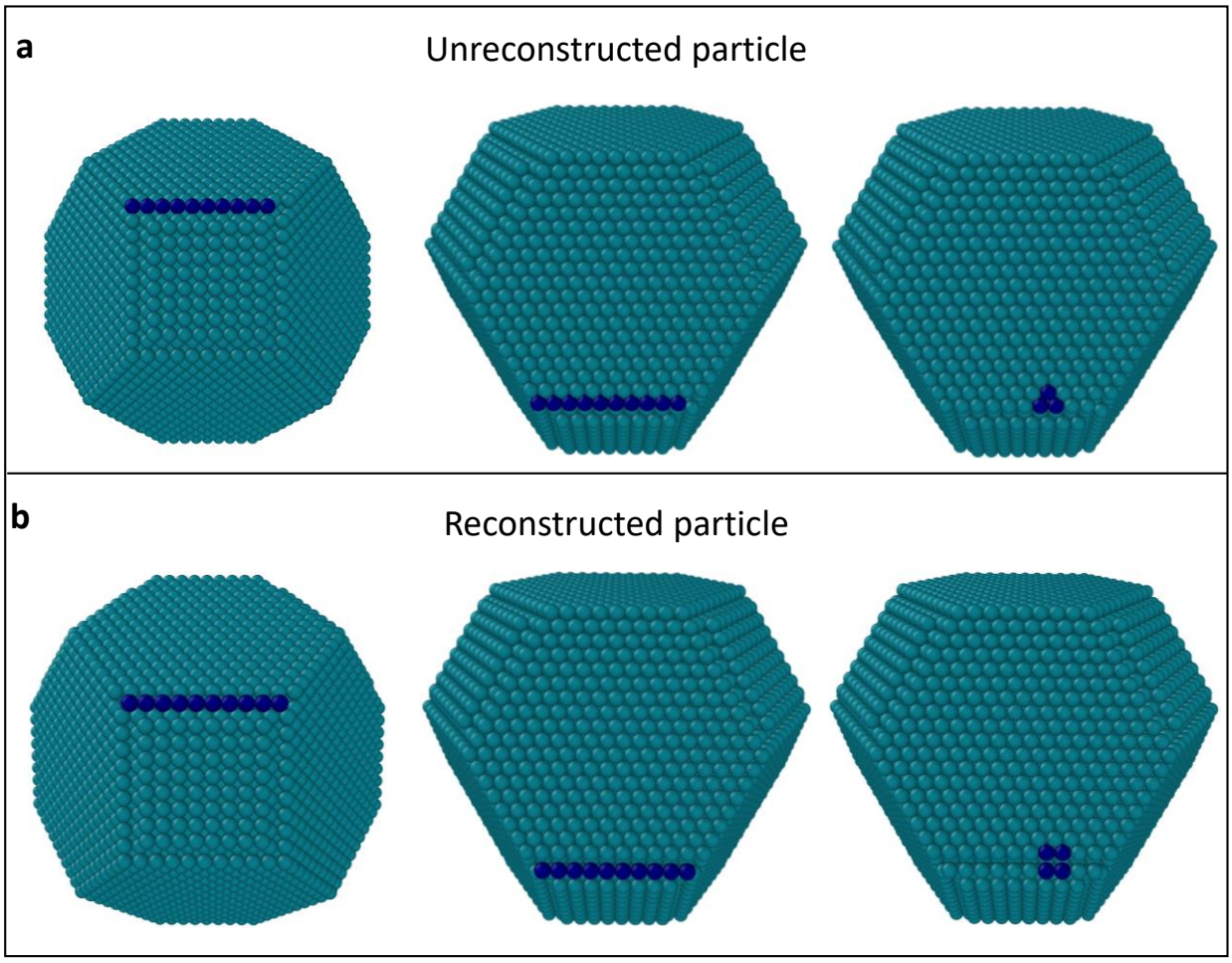

Supplementary Figure 15.

Illustrations for the edge atoms that are involved in the reconstruction and the three-fold Rh site above the edge in the unreconstructed particle in **a** and the four-fold Rh sites above the edge of the reconstructed particle in **b**.

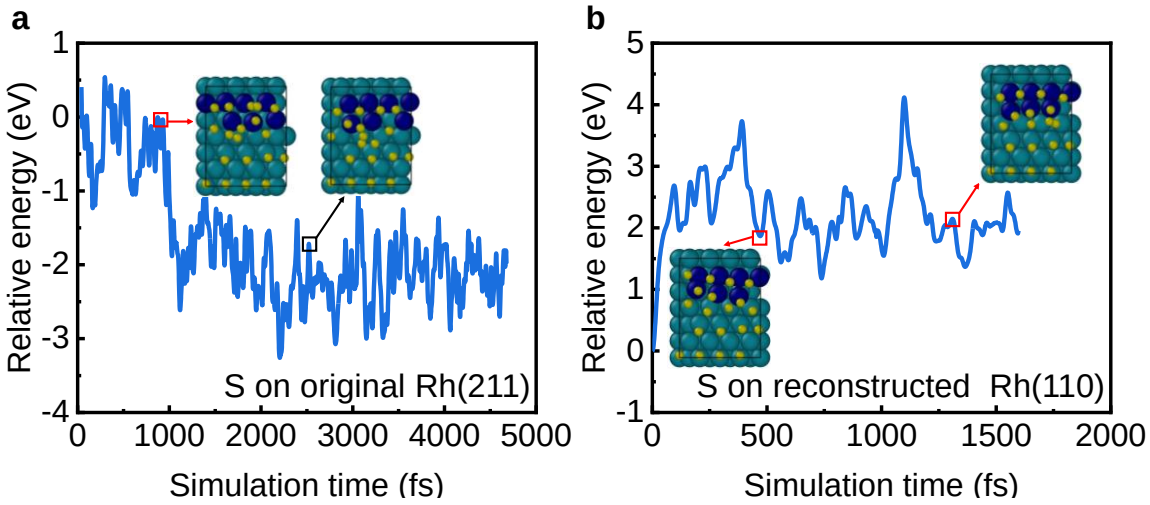

Supplementary Figure 16.

Energy changes during the transition from original Rh(211) step in **a** and reconstructed Rh(110) step in **b** in the presence of S at 850 K. The edge Rh atom close to the left boundary was removed. The trajectory of Rh and S atoms during the simulation can be found in Supplementary Movies 1 and 2. Rh atoms that were allowed to move are shown in nave and that were fixed are shown in blue, S atoms are shown in yellow in the figures and movies. Two of the Edge Rh atoms shift from the configuration of initial Rh(211) step to that of reconstructed Rh(110) step in the presence of S (**a**) while no Rh atom shifts when starting with reconstructed Rh(110) step (**b**). This suggests that adsorption of S cause the edge atoms to shift from the configuration of original Rh(211) configuration to that of the reconstructed Rh(110) which is more energetically favorable in the presence of S. Due to the local environment of the edge Rh atom which is close to the right boundary and the corner site created by removal of the Rh atom, it did not shift towards the position of the Rh(110) step. The movement of the third Rh atom in (**a**) was further investigated (Supplementary Fig. 19 and Movies 10–12).

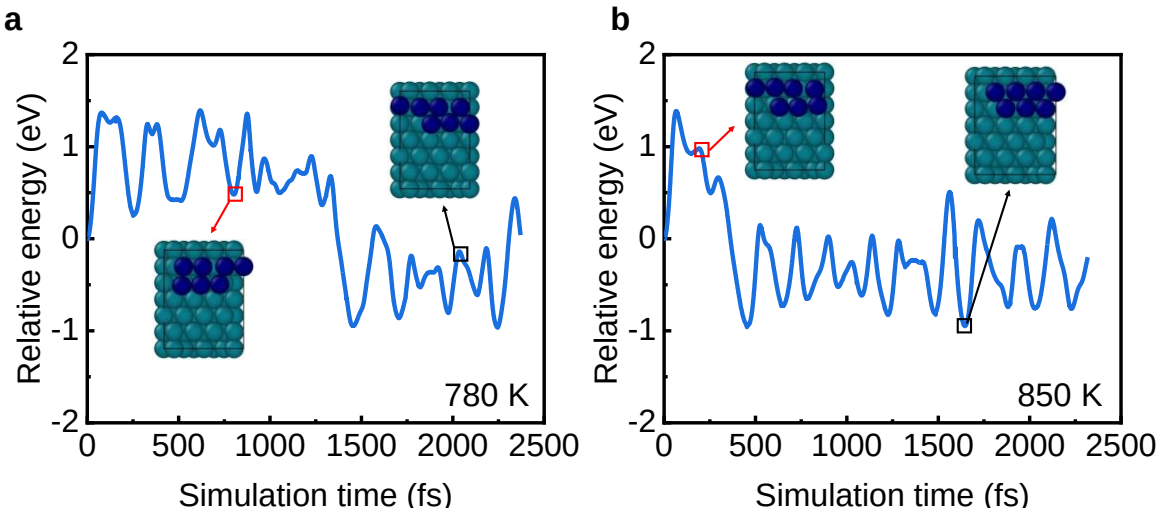

Supplementary Figure 17.

Energy changes during the transition from reconstructed Rh(110) step to original Rh(211) step in the absence of absorbates at 780 K in **a** and 850 K in **b**. The edge Rh atom close to the left boundary was removed. The trajectory of Rh atoms during the transition processes can be found in Supplementary Movies 3 and 4. Rh atoms that were allowed to move are shown in nave and that were fixed are shown in blue in the figures and movies. The transition at 780 K occurs at around 1450 fs while it occurs at 500 fs in the case of 850 K, suggesting that the reconstruction of Rh step is temperature dependent.

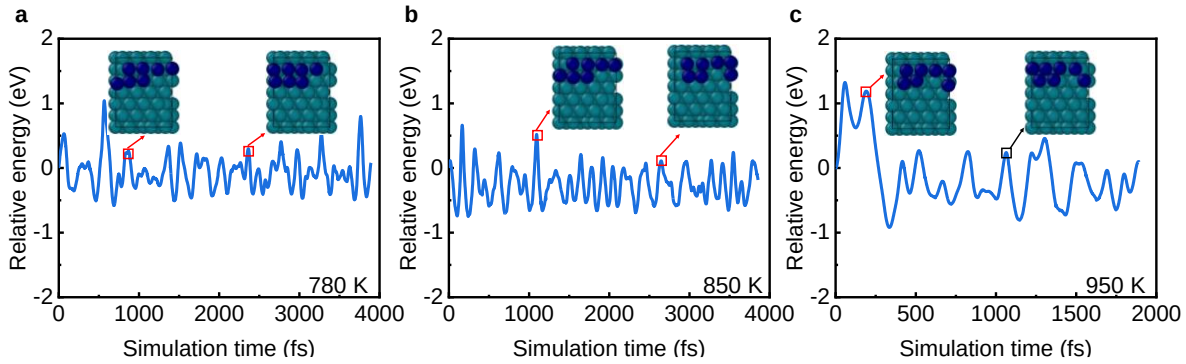

Supplementary Figure 18.

Energy changes during the transition from reconstructed Rh(110) step to original Rh(211) step in the absence of absorbates at 780 K in **a**, 850 K in **b**, and 950 K in **c**. The edge Rh atom close to the right boundary was removed. The trajectory of Rh atoms during transition processes can be found in Supplementary Movies 5–7. Rh atoms that were allowed to move are shown in nave and that were fixed are shown in blue in the figures and movies. No transition from reconstructed Rh(110) step to original Rh(211) step occurs at 780 K and 850 K (**a** and **b**). The transition occurs when further increasing the simulation temperature to 950 K (**c**). The transition occurs at 780 K and 850 K when the edge Rh atom close to the left boundary was removed (Supplementary Fig. 17). This suggests that the temperature dependence is also influence by the step configuration.

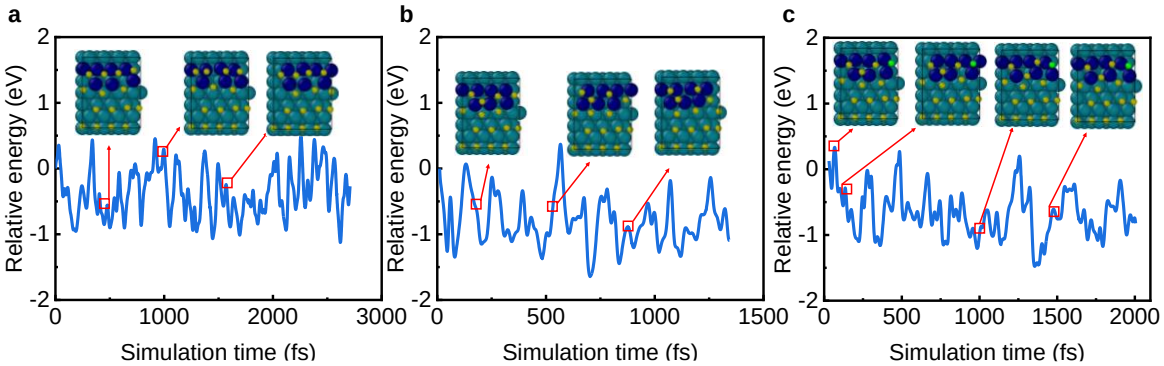

Supplementary Figure 19.

Energy changes during the AIMD simulation of taking the 2600th step in Supplementary Fig. 16**a** as initial structure and **a,** remove the three S atoms that desorbed from the Rh surface; **b,** further manually move the edge Rh atom that sits close to the right boundary to the configuration of reconstructed Rh(110) step; **c,** further fix the S atom at the right corner (green in **c**). The trajectory of Rh and S atoms during transition processes can be found in Supplementary Movies 10–12. Rh atoms that were allowed to move are shown in nave and those that were fixed are shown in blue, S atoms are shown in yellow and the S atom at the right corner that was further fixed is shown in green in the figures and movies. After removal of the three S atoms that desorbed from the Rh surface, the two edge Rh atoms close to the left boundary can be stabilized at the Rh(110) configuration while the Rh atom close to the right boundary stays at the initial position which is a corner site created by the removal of Rh atom (**a**). Further manually push the Rh atom to the Rh(110) configuration makes the corner site free for the S which leaded to the movement of all three edge Rh atoms to the Rh(211) configuration (**b**). This is supported by no transition to Rh(211) configuration by further fixation of the S atom close to the corner site (**c**). This suggests that the more under-coordinated corner site is stable for both Rh and S. The stable positions of Rh atoms at the step edge are in dynamic equilibrium and are influenced by S adsorption, S coverage, Rh neighbors (presence of Rh vacancy), as well as S positions.

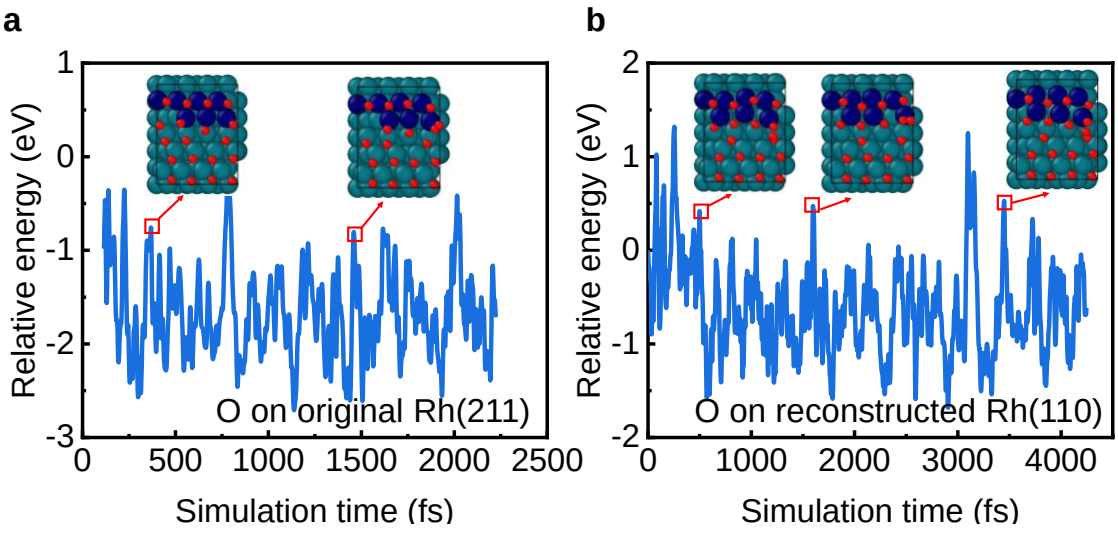

Supplementary Figure 20.

Energy changes during the transition from original Rh(211) step in **a** and reconstructed Rh(110) step in the presence of O in **b** at 850 K. The edge Rh atom close to the left boundary was removed. The trajectory of Rh and O atoms during transition processes can be found in Supplementary Movies 8 and 9. Rh atoms that were allowed to move are shown in nave and that were fixed are shown in blue, O atoms are shown in red in the figures and movies. The adsorption of O on the original Rh(211) and reconstructed Rh(110) do not cause edge Rh atoms shift away from the initial equilibrium position. Only the edge Rh atom close to the right boundary on the reconstructed Rh(110) step shifts back and forth during the simulation, however, the energy of the whole system just fluctuates around the initial energy level (**b**). This suggests that adsorption of O does not cause one-way reconstruction of Rh steps.

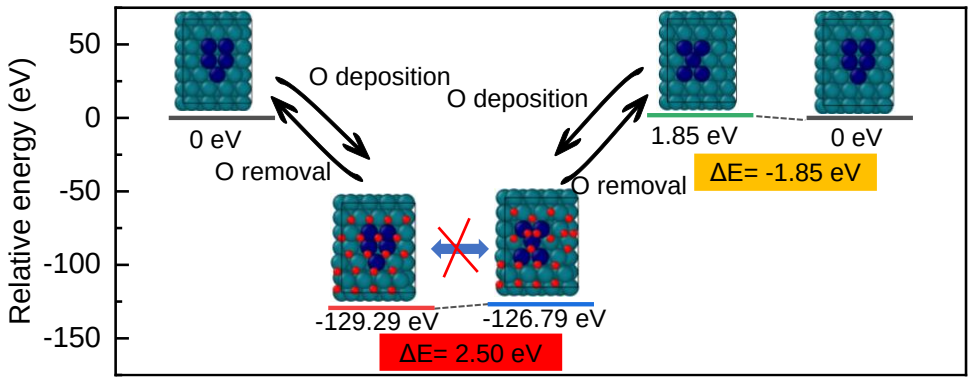

Supplementary Figure 21.

Energy diagram during O deposition and removal on Rh surface. No transition between O covered original Rh(211) step and reconstructed Rh(110) step, this was confirmed by the AIMD simulations shown in Supplementary Fig. 20, and Movies 8 and 9.

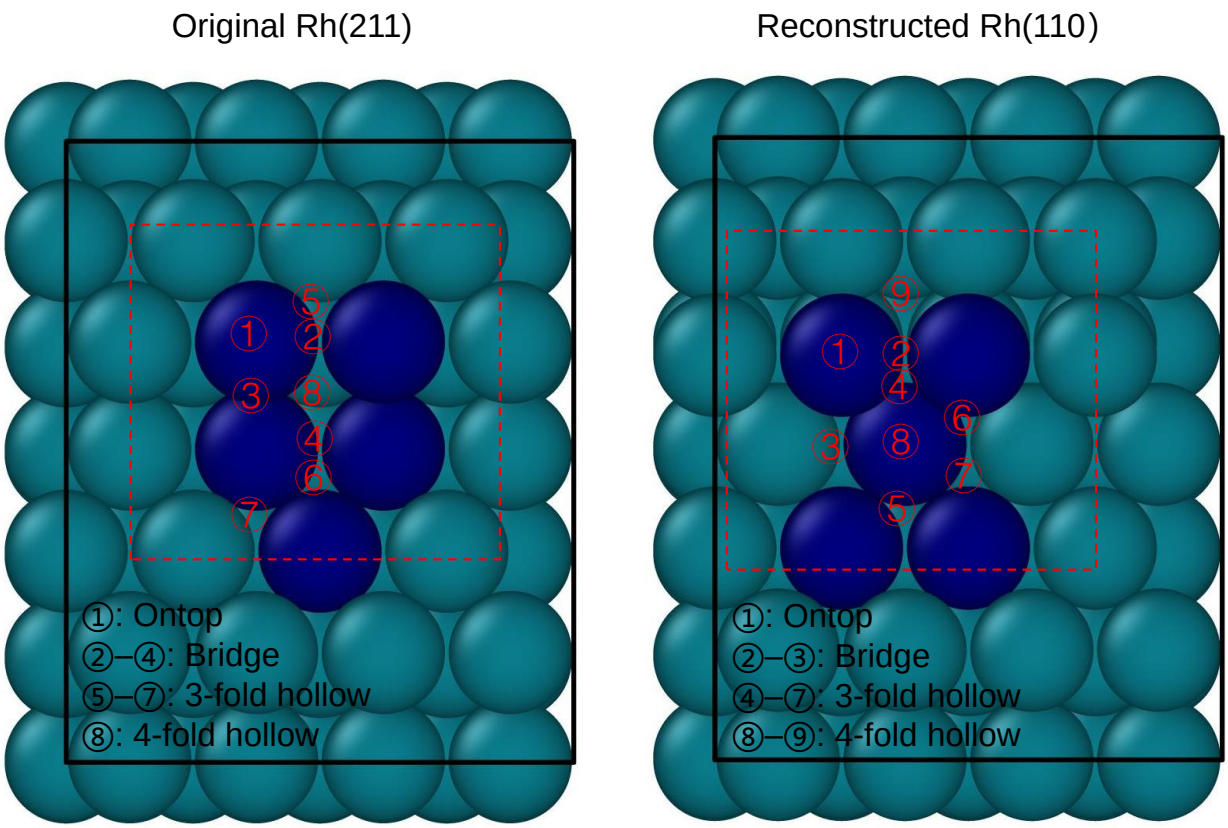

Supplementary Figure 22.

Illustration for the calculated adsorption sites on original Rh(211) step and reconstructed Rh(110) step. ①–⑧ in the original Rh(211) represent the ontop, edge bridge 1, edge bridge 2, edge bridge 3, 3-fold hollow 1, 3-fold hollow 2, 3-fold hollow 3, and 4-fold hollow sites respectively at the original Rh(211) step. ①–⑨ in the reconstructed Rh(110) represent the ontop, edge bridge 1, edge bridge 2, 3-fold hollow 1, 3-fold hollow 2, 3-fold hollow 3, 3-fold hollow 4, 4-fold hollow, and reconstructed 4-fold hollow sites respectively at the reconstructed Rh(110) step. The adsorption energies of O, S, and CH_4 on the two types of steps are listed in Supplementary Table 2. The most stable adsorption site for O, S, and CH_4 on the original Rh(211) step are the edge bridge 1 (②), 4-fold hollow (⑧), and top (①) sites respectively, and that on the reconstructed Rh(110) step are edge bridge 1 (②), reconstructed 4-fold hollow (⑨), and top (①) respectively. Similar conclusion for S adsorption on Rh(211) step had been found by previous works[1,2].

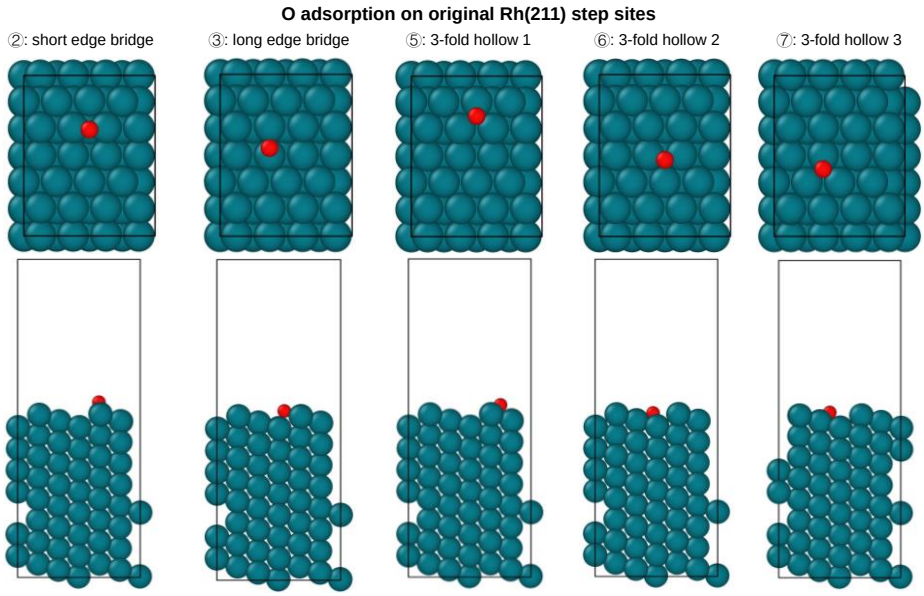

Supplementary Figure 23.

Configurations of O adsorbed on the original Rh(211) step sites at front (top panel) and right (lower panel) views. The corresponding adsorption energies are listed in Supplementary Table 2. The illustrations for the sites can be found in Supplementary Fig. 22. Rh atoms are shown in blue and O atom is shown in red.

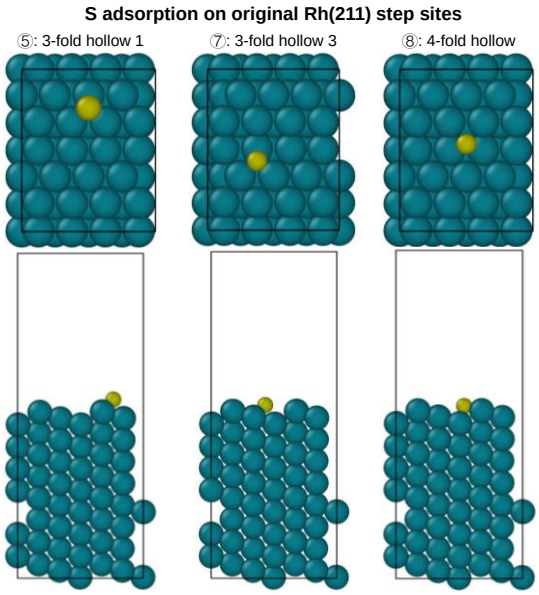

Supplementary Figure 24.

Configurations of S adsorbed on the original Rh(211) step sites at front (top panel) and right (lower panel) views. The corresponding adsorption energies are listed in Supplementary Table 2. The illustrations for the sites can be found in Supplementary Fig. 22. Rh atoms are shown in blue and S atom is shown in yellow.

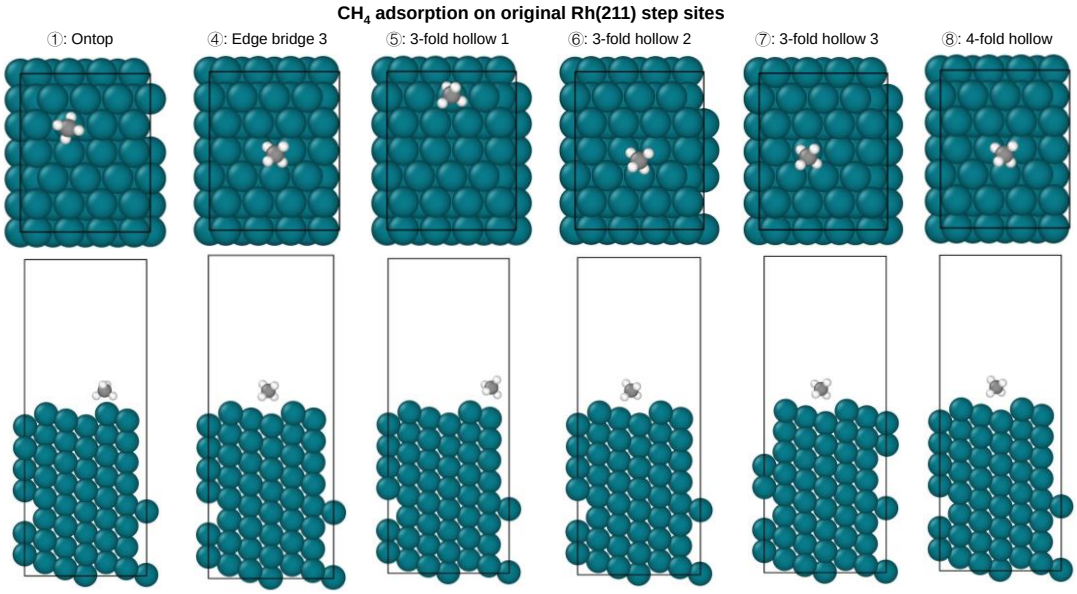

Supplementary Figure 25.

Configurations of CH_4 adsorbed on the original Rh(211) step sites at front (top panel) and right (lower panel) views. The corresponding adsorption energies are listed in Supplementary Table 2. The illustrations for the sites can be found in Supplementary Fig. 22. Rh atoms are shown in blue, H atoms are shown in white, and C atom is shown in gray.

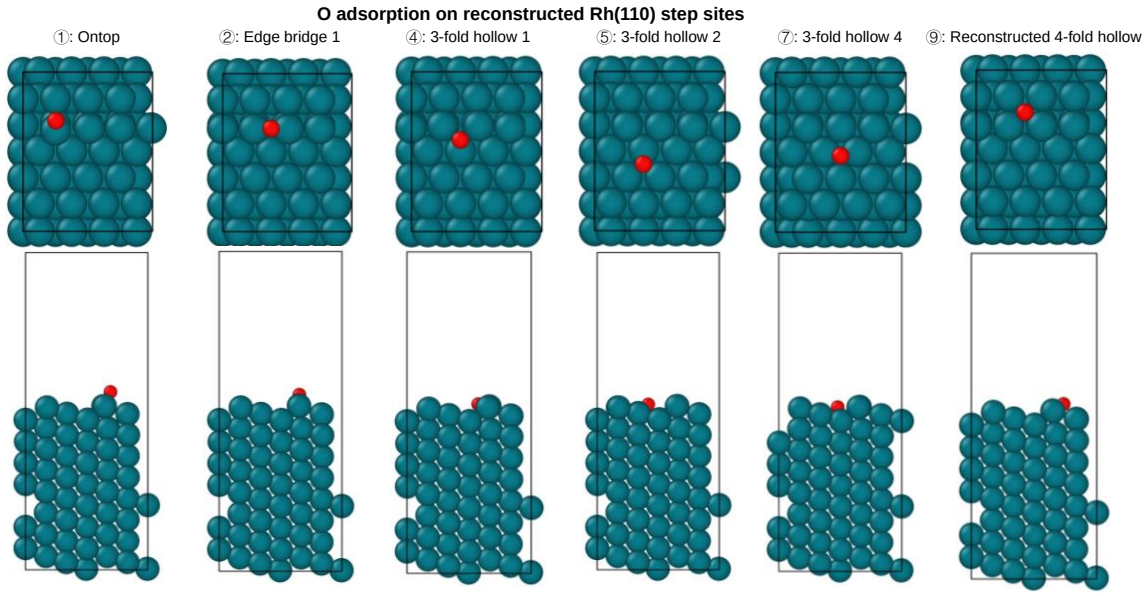

Supplementary Figure 26.

Configurations of O adsorbed on the reconstructed Rh(110) step sites at front (top panel) and right (lower panel) views. The corresponding adsorption energies are listed in Supplementary Table 2. The illustrations for the sites can be found in Supplementary Fig. 22. Rh atoms are shown in blue and O atom is shown in red.

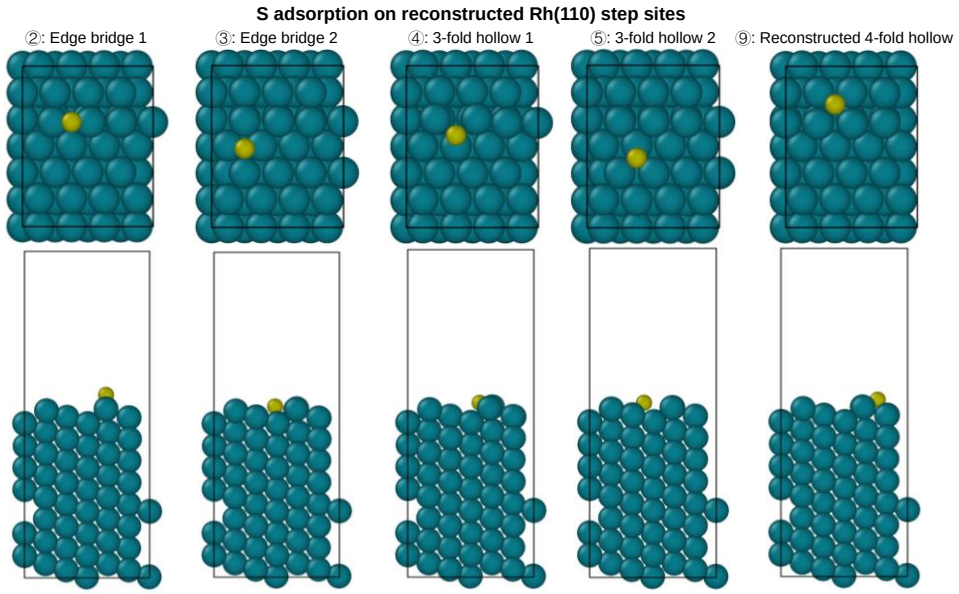

Supplementary Figure 27.

Configurations of S adsorbed on the reconstructed Rh(110) step sites at front (top panel) and right (lower panel) views. The corresponding adsorption energies are listed in Supplementary Table 2. The illustrations for the sites can be found in Supplementary Fig. 22. Rh atoms are shown in blue and S atom is shown in yellow.

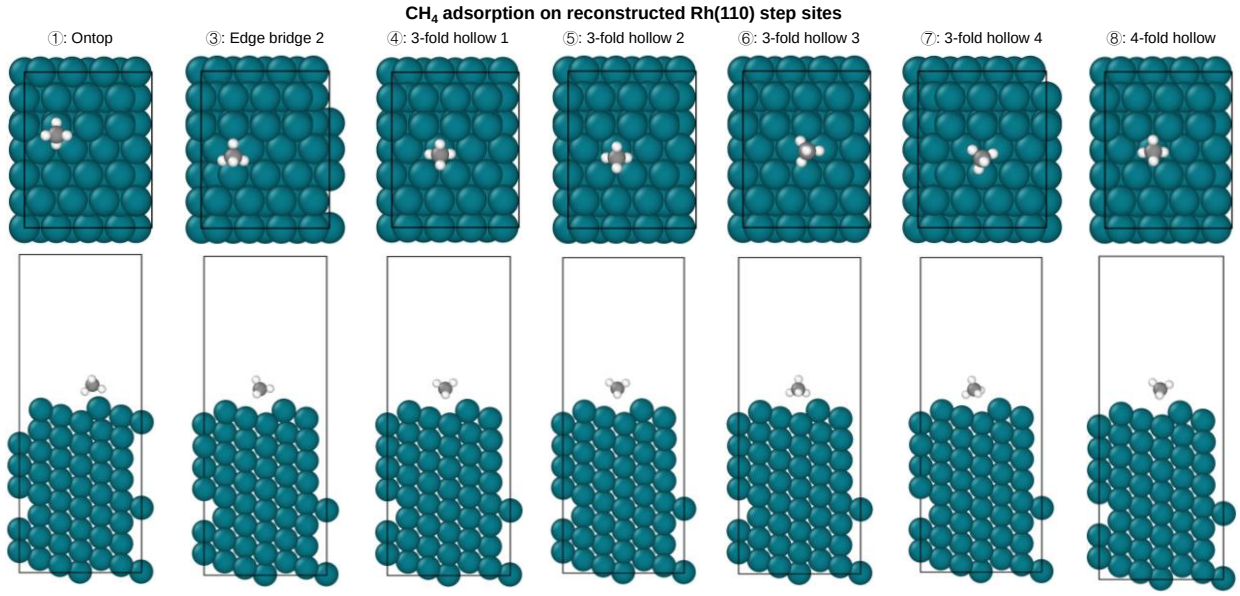

Supplementary Figure 28.

Configurations of CH_4 adsorbed on the reconstructed Rh(110) step sites at front (top panel) and right (lower panel) views. The corresponding adsorption energies are listed in Supplementary Table 2. The illustrations for the sites can be found in Supplementary Fig. 22. Rh atoms are shown in blue, H atoms are shown in white, and C atom is shown in gray.

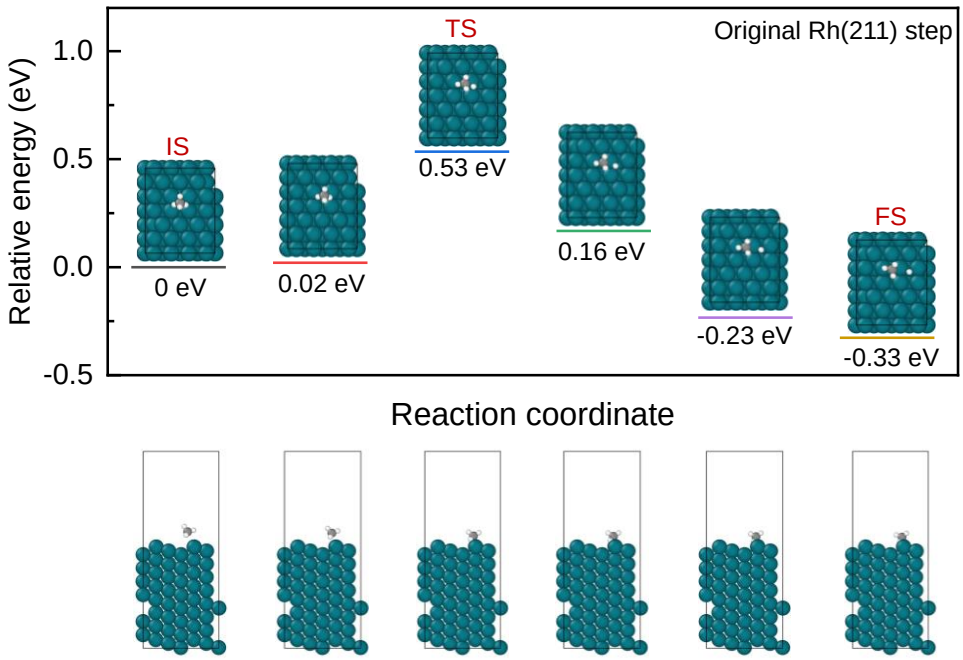

Supplementary Figure 29.

The reaction process of CH_4 dissociation on original Rh(211) step during NEB calculation and the energy change relative to the initial state. The top views of the states are show in the intersections inside the energy diagram and the corresponding right views are shown in the lower panel. Rh atoms are shown in blue, C atom is shown in gray, and H atoms are shown in white. IS, TS, and FS in the figures represent the initial state, transition state, and final state respectively. The activation barrier of CH_4 dissociation on the original Rh(211) step is then calculated to be 0.53 eV. The transition state calculation for CH_4 dissociation on the original Rh(211) step was carried out on the edge bridge 1 site (Supplementary Fig. 22) even though the most stable adsorption sites for CH_4 was found to be the ontop site since no reaction pathway was found on the ontop site (Supplementary Fig. 22, 25 and Table 2). It suggests that the most stable adsorption site is so stable that the CH_4 molecule moves to the less stable site to dissociate.

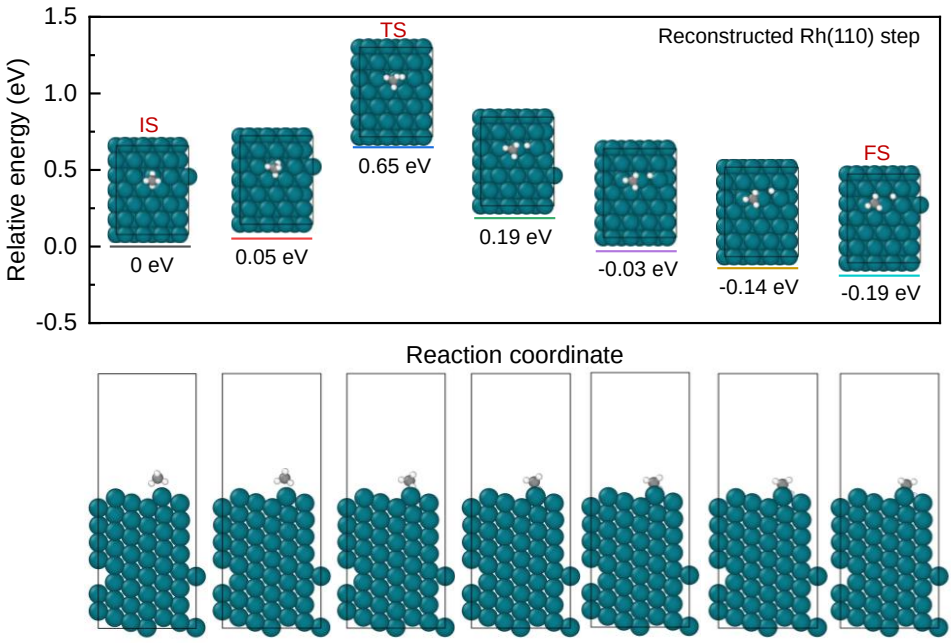

Supplementary Figure 30.

The reaction process of CH_4 dissociation at the Ontop site on reconstructed Rh(110) step during NEB calculation and the energy change relative to the initial state. The Ontop site was found to be the most stable site for CH_4 adsorption on the reconstructed Rh(100) step (Supplementary Fig. 22, 28 and Table 2). The top views of the states are show in the intersections inside the energy diagram and the corresponding right views are shown in the lower panel. Rh atoms are shown in blue, C atom is shown in gray, and H atoms are shown in white. IS, TS, and FS in the figures represent the initial state, transition state, and final state respectively. The activation barrier of CH_4 dissociation on the reconstructed Rh(110) step is then calculated to be 0.65 eV.

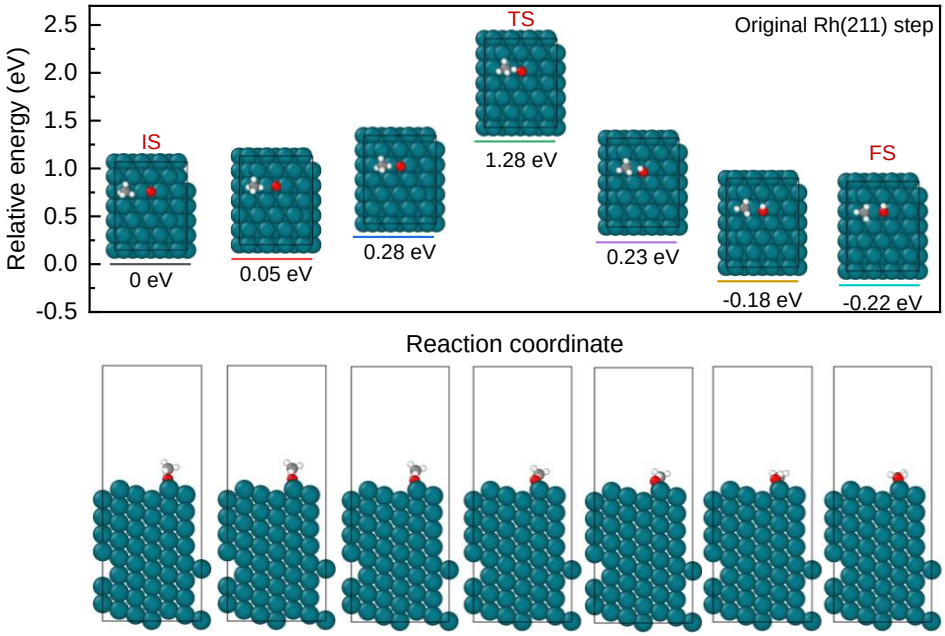

Supplementary Figure 31.

The reaction process of CH_4 dissociation on O adsorbed original Rh(211) step during NEB calculation and the energy change relative to the initial state. The initial and final states were confirmed by the adsorption energy calculations as shown in Supplementary Fig. 22, 23, 25, and Table 2. The top views of the states are show in the intersections inside the energy diagram and the corresponding right views are shown in the lower panel. Rh atoms are shown in blue, O atom is shown in red, C atom is shown in gray, and H atoms are shown in white. IS, TS, and FS in the figures represent the initial state, transition state, and final state respectively. The activation barrier of CH_4 dissociation on the O adsorbed original Rh(211) step is then calculated to be 1.28 eV.

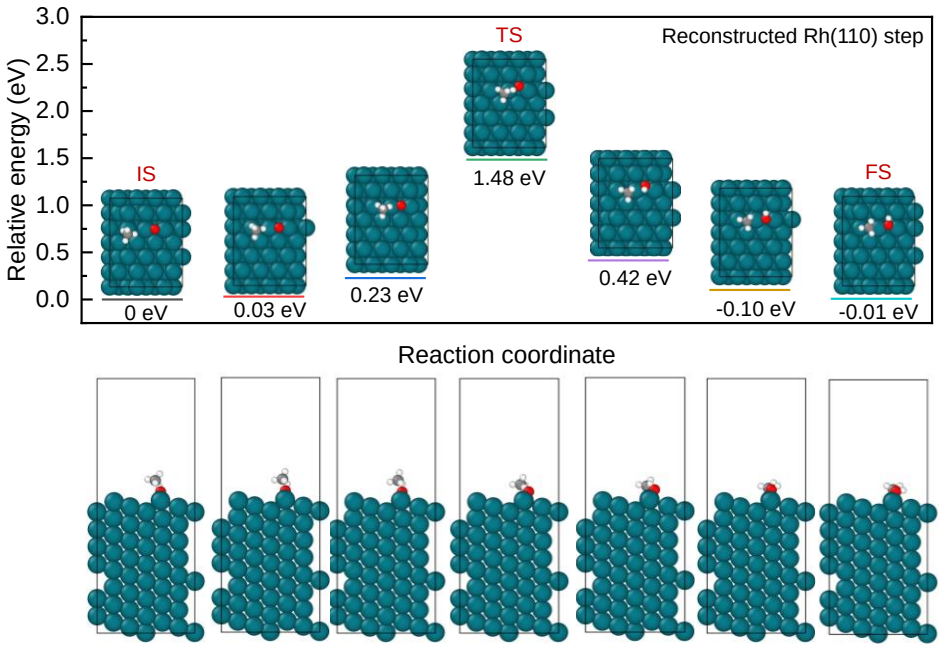

Supplementary Figure 32.

The reaction process of CH_4 dissociation on O adsorbed reconstructed Rh(110) step during NEB calculation and the energy change relative to the initial state. The initial and final states were confirmed by the adsorption energy calculations as shown in Supplementary Fig. 22, 26, 28, and Table 2. The top views of the states are show in the intersections inside the energy diagram and the corresponding right views are shown in the lower panel. Rh atoms are shown in blue, O atom is shown in red, C atom is shown in gray, and H atoms are shown in white. IS, TS, and FS in the figures represent the initial state, transition state, and final state respectively. The activation barrier of CH_4 dissociation on the O adsorbed reconstructed Rh(110) step is then calculated to be 1.48 eV.

Supplementary Table 1.

Surface energies of Rh with and without S adsorption. The absolute values of the surface energies of Rh with S would depend on the reference state of S, so in the table, we have reported shifted energies, such that the surface energy of the (111) termination is identical for Rh with and without S. The (111) surface energy values are therefore in italics to indicate the reference state and the (100) is in bold to highlight the largest decrease in surface energy upon S adsorption.

Miller plane	Surface energy Rh (eV/Å^2)	Change in Surface energy relative to (111) Rh (0.5 ML S) (eV/Å^2)	Surface energy Rh (0.5 ML S) (eV/Å^2)
(111)	0.153	*0*	*0.153*
(100)	0.168	**-0.080**	**0.089**
(110)	0.170	-0.031	0.139
(211)	0.166	-0.028	0.138

Supplementary Table 2.

Adsorption energies of O, S, CH_4 on the preferred Rh sites of original Rh(211) and reconstructed Rh(110) steps. For the sites that are stable for O, S, and CH_4, the corresponding adsorption configurations are shown in Supplementary Figs. 22–28. The strongest adsorption energies on the original Rh(211) and reconstructed Rh(110) are in bold to highlight the most stable sites for O, S, and CH_4 adsorptions.

Adsorption sites of Rh steps[a]			Adsorption energy (eV)		
			O	S	CH_4
Original Rh(211)	①	Ontop	/	/	**-0.32**
	②	Edge bridge 1	**-7.16**	/	/
	③	Edge bridge 2	-6.53	/	/
	④	Edge bridge 3	/	/	-0.25
	⑤	3-fold hollow 1	-7.00	-6.81	-0.23
	⑥	3-fold hollow 2	-6.64	/	-0.26
	⑦	3-fold hollow 3	-6.71	-6.70	-0.25
	⑧	4-fold hollow	/	**-6.94**	-0.26
Reconstructed Rh(110)	①	Ontop	-6.16	/	**-0.34**
	②	Edge bridge 1	**-7.35**	-6.51	/
	③	Edge bridge 2	/	-6.78	-0.27
	④	3-fold hollow 1	-7.06	-6.89	-0.25
	⑤	3-fold hollow 2	-6.63	-6.63	-0.25
	⑥	3-fold hollow 3	/	/	-0.29
	⑦	3-fold hollow 4	-6.51	/	-0.27
	⑧	4-fold hollow	/	/	-0.25
	⑨	Reconstructed 4-fold hollow	-7.08	**-7.37**	/

[a]: The illustrations for adsorption sites is shown in Supplementary Fig. 22.

/: The diagonal represents no stable adsorption configuration on the corresponding site.

Supplementary Table 3.

Activation barriers for CH_4 dissociation on clean and O adsorbed Rh step sites from NEB calculations. The sites for CH_4 dissociation were chosen based on the adsorption energies on different sites shown in Supplementary Table 2. The corresponding configurations as well as the energy diagrams are shown in Supplementary Figs. 29–32.

Rh sites		Relative energies refer to the energy at initial state		
		E_{TS} (eV)	E_{FS} (eV)	Eact (eV)
Clean surface	Original Rh(211)	0.53	-0.33	0.53
	Reconstructed Rh(110)	0.65	-0.19	0.65
O adsorbed surface	Original Rh(211)	1.28	-0.22	1.28
	Reconstructed Rh(110)	1.48	0.01	1.48

Supplementary Note 1.

Sulfur coverage calculation. Sulfur coverage is calculated by the molar ratio of adsorbed/released sulfur to the molar of surface Rh estimated by the size of the nanoparticle determined by TEM (Eq. 1).

$$Sulfur\ coverage = \frac{N_S}{N_{Rh,m}} \quad (1)$$

N_S is the number of released sulfur calculated by the integration of the sulfur peak above the inlet concentration when stopping the CH_4 feeding in Fig. 1d in the main text. $N_{Rh,S}$ is the number of surface Rh atoms for a Rh nanoparticle with the diameter of d_p calculated according to Eq. 2 using the occupied area per Rh atom (a_{Rh}=7.58 $Å^2$) by assuming equal contribution from fcc (111), (100), and (110) crystal planes to the Rh surface.

$$N_{Rh,S} = \frac{SSA * m_{Rh}}{a_{Rh}} = \frac{6 * m_{Rh}}{a_{Rh} * \rho_{Rh} * d_P} \quad (2)$$

SSA: specific surface area of Rh, m^2/g; m_{Rh}: mass of Rh, g; ρ_{Rh}: gravimetric density of Rh, $1.24*10^7$ g/m^3.

Supplementary Note 2.

Calculations for the step concentration vs particle diameters based on Wulff principle. Based on our DFT calculations Wulff constructed nanoparticles have step sites at 2 nm but not at 1.5 nm so we have assumed a linearly increasing step concentration in this narrow range. As the steps occur at the particle edges in the Wulff constructed nanoparticles the concentration of step sites will follow the fraction of edge sites which scales with the inverse particle diameter. This is in good agreement with the analyses of Ishikawa et al.[3] although our updated DFT calculations predict the emergence of step sites at a smaller particle diameter. The normalized step concentration f_{step} as a function of particle size was calculated according to Eq.3, where d is the particle diameter (The detailed calculation shown in Supplementary Sheet 1):

$$f_{step} = \begin{cases} 0 \text{ for } d < 1.5\ nm \\ 200d - 300 \text{ for } 1.5 < d < 2\ nm \\ \dfrac{200}{d} \text{ for } d > 2\ nm \end{cases} \quad (3)$$

Supplementary Note 3.

Data illustration for the theoretical calculations. The models for DFT and AIMD calculations were built and viewed using Atomic Simulation Environment (ASE)[4], the adsorption and reaction configuration pictures and the AIMD videos are visualized using ASE and Visualization for Electronic and Structural Analysis (VESTA)[5], and rendered using OVITO[6]. The Wulff-constructed Rh nanoparticle was built using the crystallographic tool[7] for the construction of nanoparticles with the Crystallographic Information File (cif) downloaded from The Inorganic Crystal Structure Database (ICSD) database[8] and surface energies of different Rh facets provided by mavrl: crystalium - Materials Virtual Lab[9].

Description for Supplementary Movie 1.

Transition from Rh(211) step to reconstructed Rh(110) step at 850 K with S adsorption when the edge Rh atom and S atom at the left boundary were removed. Rh atoms that were allowed to move are shown in nave and that were fixed are shown in blue, S atoms were shown in yellow. The video framerate rate was set to be 60 frames per second (1 s = 60 fs).

Description for Supplementary Movie 2.

No transition from reconstructed Rh(110) step at 850 K with S adsorption when the edge Rh atom and S atom at the left boundary were removed. Rh atoms that were allowed to move are shown in nave and that were fixed are shown in blue, S atoms were shown in yellow. The video framerate rate was set to be 60 frames per second (1 s = 60 fs).

Description for Supplementary Movie 3.

Transition from reconstructed Rh(110) step to Rh(211) step at 780 K when the edge Rh atom at the left boundary was removed. Rh atoms that were allowed to move are shown in nave and that were fixed are shown in blue. The video framerate rate was set to be 60 frames per second (1 s = 60 fs).

Description for Supplementary Movie 4.

Transition from reconstructed Rh(110) step to Rh(211) step at 850 K when the edge Rh atom at the left boundary was removed. Rh atoms that were allowed to move are shown in nave and that were fixed are shown in blue. The video framerate rate was set to be 60 frames per second (1 s = 60 fs).

Description for Supplementary Movie 5.

No transition of reconstructed Rh(110) step at 780 K when the edge Rh atom at the right boundary was removed. Rh atoms that were allowed to move are shown in nave and that were fixed are shown in blue. The video framerate rate was set to be 60 frames per second (1 s = 60 fs).

Description for Supplementary Movie 6.

No transition of reconstructed Rh(110) step at 850 K when the edge Rh atom at the right boundary was removed. Rh atoms that were allowed to move are shown in nave and that were fixed are shown in blue. The video framerate rate was set to be 60 frames per second (1 s = 60 fs).

Description for Supplementary Movie 7.

Transition from reconstructed Rh(110) step to Rh(211) step at 950 K when the edge Rh atom at the right boundary was removed. Rh atoms that were allowed to move are shown in nave and that were fixed are shown in blue. The video framerate rate was set to be 60 frames per second (1 s = 60 fs).

Description for Supplementary Movie 8.

No transition of Rh(211) step at 850 K with O adsorption when the edge Rh atom and O atom at the left boundary were removed. Rh atoms that were allowed to move are shown in nave and that were fixed are shown in blue, O atoms were shown in red. The video framerate rate was set to be 60 frames per second (1 s = 60 fs).

Description for Supplementary Movie 9.

Rh atom movement of reconstructed Rh(110) step at 850 K with O adsorption when the edge Rh atom and O atom at the left boundary were removed. Rh atoms that were allowed to move are shown in nave and that were fixed are shown in blue, O atoms were shown in red. The video framerate rate was set to be 60 frames per second (1 s = 60 fs).

Description for Supplementary Movie 10.

AIMD simulation using the 2600th step of Movie 1 as initial structure with the S atoms that desorbed from surface being removed. Rh atoms that were allowed to move are shown in nave and that were fixed are shown in blue, S atoms were shown in yellow. The video framerate rate was set to be 60 frames per second (1 s = 60 fs).

Description for Supplementary Movie 11.

AIMD simulation using the 2600th step of Movie 1 as initial structure with the S atoms that desorbed from surface being removed and the most right Rh atom being manually pushed to the configuration of reconstructed Rh(110) site. Rh atoms that were allowed to move are shown in nave and that were fixed are shown in blue, S atoms are shown in yellow. The video framerate rate was set to be 60 frames per second (1 s = 60 fs).

Description for Supplementary Movie 12.

AIMD simulation using the 2600th step of Movie 1 as initial structure with the S atoms that desorbed from surface being removed, the most right Rh atom being manually pushed to the configuration of reconstructed Rh(110) site, and the S atom at the top right corner was fixed. Rh atoms that were allowed to move are shown in nave and that were fixed are shown in blue, S atoms are shown in yellow, the S atom that was fixed during the simulation is shown in green. The video framerate rate was set to be 60 frames per second (1 s = 60 fs).

Supplementary References

1. Bernard Rodríguez, C. R. & Santana, J. A. Adsorption and diffusion of sulfur on the (111), (100), (110), and (211) surfaces of FCC metals: Density functional theory calculations. *J. Chem. Phys.* **149**, 204701 (2018).
2. McAllister, B. & Hu, P. A density functional theory study of sulfur poisoning. *J. Chem. Phys.* **122**, 084709 (2005).
3. Ishikawa, A., Doi, T. & Nakai, H. Catalytic performance of Ru, Os, and Rh nanoparticles for ammonia synthesis: A density functional theory analysis. *J. Catal.* **357**, 213–222 (2018).
4. Hjorth Larsen, A. *et al.* The atomic simulation environment - A Python library for working with atoms. *J. Phys. Condens. Matter* **29**, 273002 (2017).
5. Momma, K. & Izumi, F. VESTA 3 for three-dimensional visualization of crystal, volumetric and morphology data. *J. Appl. Crystallogr.* **44**, 1272–1276 (2011).
6. Stukowski, A. Visualization and analysis of atomistic simulation data with OVITO-the Open Visualization Tool. *Model. Simul. Mater. Sci. Eng.* **18**, 015012 (2010).
7. Chatzigoulas, A., Karathanou, K., Dellis, D. & Cournia, Z. NanoCrystal: A web-based crystallographic tool for the construction of nanoparticles based on their crystal habit. *J. Chem. Inf. Model.* **58**, 2380–2386 (2018).
8. Singh, H. P. Determination of thermal expansion of germanium, rhodium and iridium by X-rays. *Acta Crystallogr. Sect. A* **24**, 469–471 (1968).
9. Tran, R. *et al.* Data Descriptor: Surface energies of elemental crystals. *Sci. Data* **3**, 160080 (2016).